GNSS Multipath & Jamming Mitigation Using High Mask Angle Antennas and Multiple Constellations

Liang Heng, *Member, IEEE*, Todd Walter, Per Enge, *Fellow, IEEE*, and Grace Xingxin Gao, *Member, IEEE*

***Abstract*—Multipath and jamming interference affects accuracy, availability, and continuity of global navigation satellite systems (GNSS). The U.S. Global Positioning System (GPS) and the Russian GLONASS are being joined by the European Galileo and the Chinese BeiDou. An increasing number of satellites in multiple constellations enable users to use high mask angle antennas (HMAAs) to mitigate interference signals coming from a low elevation angle. This paper studies the optimal antenna mask angle that maximizes the suppression of interference but still maintains the performance of a single constellation with a low mask angle antenna. The paper first proves a novel lower bound on expectation of dilution of precision (DOP) and derives closed-form formulas that relate the lower bound to antenna mask angle and number of satellites. Then, through extensive simulations, a variety of optimal mask angles are obtained with respect to different constellation settings, different DOP metrics, and different assumptions of range accuracy. The numerical results highly agree with our theory. Both of them show that two constellations can match performance of one with 5–14° higher mask, and three constellations can match performance of one with 11–23° higher mask, depending on the DOP metric and the range error model used. The numerical results also show that using HMAAs is more beneficial to users interested in positioning accuracy than users interested in time transfer accuracy.**

***Index Terms*—Interference, multipath, jamming, antenna, mask angle, dilution of precision (DOP), lower bound, GPS, global navigation satellite system (GNSS), multiple constellations**

I. Introduction

LOCATION awareness is crucial in transportation systems to enhance efficiency, safety, and flexibility while reducing congestion and pollution [1], [2]. The Global Positioning System (GPS) has been widely used to position automobiles, trains, ships, and airplanes [3]–[5]. As a radionavigation system, GPS can be impaired by radio frequency (RF) interference such as *multipath* and *jamming*. Multipath interference occurs when the GPS signal is reflected or diffracted from surrounding terrain such as ground, buildings, foliage, hills, and even sea surface [6]. Multipath is one of the dominant error sources in GPS pseudorange measurements, especially for differential positioning in high accuracy applications [7]. While multipath interference mainly affects GPS accuracy performance, jamming interference affects availability and continuity performance. Jamming is attributable to a nearby transmitter which, intentionally or unintentionally, emit RF signals overlapping GPS frequencies. Since the power of GPS signals received on the Earth is as low as 10^{-16} W, even below the thermal noise floor [8], a low-power GPS jammer can easily affect GPS receivers in a considerable area [5], [9]. As transportation systems come to rely more and more on GPS, it would be of great importance to harden GPS receivers against multipath and jamming interference.

Most of previous work treated multipath and jamming as two separated problems. For multipath mitigation, existing approaches can be classified into three groups: antenna-based, tracking loop-based, and extra information-based. The first group includes the use of special antennas [10]–[12] or multi-antenna arrays [13], [14]. The tracking loop-based approaches focus on how to improve code tracking loops. Significant work includes narrow correlator spacing [15] and strobe & edge correlator [16]. The extra information-based methods utilize other information generated by the receiver or external to the GPS subsystems, such as carrier phase [17], signal-to-noise ratio [18], and maps with elevation information [19].

A variety of methods have been proposed to help GPS receivers counter jamming interference. For interference signals known to be sparse in the time and/or frequency domains, pre-correlation excisers can suppress interference signals through time-frequency filtering [20]–[22]. Unfortunately, these excisers are not very effective when interference signals are not sparse. Antenna arrays represent a promising approach to suppressing jamming signals regardless of their sparsity in time and frequency domains. An antenna array can form beams to satellites and steer nulls to jammers, greatly improving the signal to interference plus noise ratio [23]–[25]. In practice, antenna arrays suffer from issues such as the bulky size, complex structure, computationally intensive receiver processing, and time-varying biases introduced by spatial and temporal filtering [26]. These drawbacks limit the use of antenna arrays, especially for vehicular applications.

The development of other global navigation satellite systems (GNSS), i.e., the Russian Global'naya Navigatsionnaya Sputnikovaya Sistema (GLONASS), the European Galileo, and the Chinese Compass, offers a new opportunity of using high mask angle antennas (HMAAs) to counter RF interference [27]. Antenna mask angle, also referred to as cutoff angle, is a parameter in GNSS antenna design defining the elevation below which RF signals will be considerably attenuated. It should not be confused with the parameter "mask angle" or "cutoff angle" in receiver configuration for excluding low-elevation satellites from position solution.

The HMAA method is based on the fact that multipath reflectors and jamming sources are mostly on the ground. A HMAA can suppress interference and GNSS signals com-

Authors' address: L. Heng and G. Gao, Department of Aerospace Engineering, University of Illinois at Urbana-Champaign, Urbana, IL 61801, (E-mail: {heng, gracegao}@illinois.edu); T. Walter and P. Enge, Department of Aeronautics and Astronautics, Stanford University, Stanford, CA 94305, (E-mail: {twalter, per.enge}@stanford.edu).

ing from low elevation angles. With an increased number of satellites in multiple constellations, the receiver can still comply with the performance requirements defined for a single constellation with a low mask angle antenna.

A major difference between the HMAAs and existing anti-jamming antennas [10]–[12] is that the anti-multipath antennas are mostly designed for GPS-only. As a result, anti-multipath antennas have to use a low mask angle (typically 5°), and their gain pattern should have a sharp cutoff around the mask angle. The requirement of a sharp cutoff leads to large size and weight, which are unfavorable for vehicular applications. The HMAAs can use a much higher mask angle, without requiring a sharp cutoff. Therefore, an HMAA can be potentially made in the same size as an ordinary patch antenna. For instance, F. Bauregger et al. [28] have designed a dual patch antenna which can switch between two modes: wide-looking mode (low mask angle) and narrow-looking mode (high mask angle). With a 18° increase in the mask angle, the dual patch antenna obtains 10-dB advantage in rejecting signals from the horizon.

Although the use of HMAAs is an intuitive solution, and is likely to be implemented in practice [27], there is a dearth of comprehensive theoretical and numerical analyses. For example, it remains unclear how much the optimal mask angle should be. In general, the higher the mask angle, the greater the attenuation of signals from low elevation angles is. On the other hand, if the mask angle is too high, losing a large number of low-elevation satellites will affect positioning and timing performance.

The objective of this paper is to find the optimum mask angle—defined as the highest mask angle with which the performance of multiple constellations is not worse than the performance of a single constellation with a standard, low mask angle antenna. We focus on accuracy performance and employ dilution of precision (DOP) [8], [29] as a performance measure. Although there have been some prior work studying DOP using real data, simulations, or analytical methods [29]–[33], few of them have established a quantitative relationship between antenna mask angle and DOP performance. The major contributions of this paper are highlighted as follows.

- We prove a novel lower bound on the expectation of DOP.
- From the lower bound, we derive closed-form formulas that relate accuracy performance to two parameters: antenna mask angle and number of satellites.
- Our comprehensive simulations validate our theory, and also provide more insights into how the optimum mask angle varies with different DOP metrics, different range error models, and the users at different latitudes.

The rest of this paper proceeds as follows. Section II formally formulates the problem and introduces the utility functions. Section III presents our theorem of the lower bound and derives the closed-form formulas. Section IV presents simulation results of optimal mask angles. Finally, Section V concludes the paper. Proof of the theorem is provided in the Appendix.

II. Preliminaries

A. Problem formulation

The choice of mask angle is a tradeoff between robustness and performance. On one hand, as has been discussed in Section I, a higher mask angle can better suppress interference signals coming from low elevation angles. On the other hand, a higher mask angle also rejects useful signals from low elevation GNSS satellites, and thus leads to worse user-satellite geometry, which degenerates accuracy performance.

In this paper, our goal is to find the optimal antenna mask angle such that the robustness is maximized without sacrificing performance. Mathematically, it can be formulated as the following optimization problem:

$$\begin{aligned} &\text{maximize} \quad \alpha, \\ &\text{subject to} \quad u(n,\alpha) \geq u(n_0,\alpha_0). \end{aligned} \tag{1}$$

In (1), α is the mask angle for multiple constellations, which include a total of n satellites; α_0 is the mask angle for a single constellation, which includes a total of n_0 satellites; $u(n,\alpha)$ is a utility function quantifying the goodness or performance of satellite geometry. In this paper, the baseline geometry is based on a single GPS constellation of 30 satellites with a 5° mask angle, i.e., $n_0 = 30$ and $\alpha_0 = 5°$.

For most GNSS applications, the utility function $u(n,\alpha)$ is monotonically increasing with respect to n and monotonically decreasing with respect to α. Since multiple constellations contain more satellites than a single constellation, i.e., $n > n_0$, we have $u(n,\alpha_0) > u(n_0,\alpha_0)$. Therefore, there must exist $\alpha^* > \alpha_0$ such that

$$u(n,\alpha^*) = u(n_0,\alpha_0). \tag{2}$$

α^* is the optimal mask angle satisfying (1). This proves that the optimization problem (1) is always feasible, and there must exist a mask angle higher than α_0 for multiple constellations to match the baseline performance.

B. DOP metrics

When the satellites of different constellations can be assumed to have the same range accuracy, DOP simply specifies the multiplicative effect on positioning accuracy due to satellite geometry. When the satellites of different constellations cannot be assumed to have the same range accuracy performance [34]–[36], weighted DOP (WDOP), also known as KDOP [31], [37], is used in this paper to specify the multiplicative effect on positioning accuracy due to not only satellite geometry but also the range accuracy performance of different constellations.

For interoperable[1] GNSS constellations, the geometry matrix [8] of m visible satellites can be written as

$$G = \begin{pmatrix} \cos\phi_1\cos\theta_1 & \cos\phi_1\sin\theta_1 & \sin\phi_1 & -1 \\ \vdots & \vdots & \vdots & \vdots \\ \cos\phi_m\cos\theta_m & \cos\phi_m\sin\theta_m & \sin\phi_m & -1 \end{pmatrix}, \tag{3}$$

[1]Interoperablity means that the reference frames of different GNSS constellations are consistent, and the time offsets between different constellations are known [38].

where ϕ_k and θ_k are the elevation and azimuth angles of the kth satellite seen by the user, $k = 1, \ldots, m$. The covariance of positioning errors $\boldsymbol{\varepsilon}$ is given by [8]

$$\mathrm{cov}(\boldsymbol{\varepsilon}, \boldsymbol{\varepsilon}) = (G^{\mathsf{T}} \Sigma^{-1} G)^{-1}, \tag{4}$$

where $\Sigma = \mathrm{cov}(\boldsymbol{\epsilon}, \boldsymbol{\epsilon})$ is the covariance of range errors $\boldsymbol{\epsilon}$. If the range errors of different satellites can be assumed to be independent, the covariance matrix is diagonal,

$$\Sigma = \mathrm{diag}(\sigma_1^2, \ldots, \sigma_k^2). \tag{5}$$

Let σ^2 denote the nominal variance of the range errors of GPS satellites. With the weighting matrix defined as

$$W = \mathrm{diag}(\sigma_1^2/\sigma^2, \ldots, \sigma_k^2/\sigma^2), \tag{6}$$

the covariance of positioning errors can be rewritten as

$$\mathrm{cov}(\boldsymbol{\varepsilon}, \boldsymbol{\varepsilon}) = \sigma^2 (G^{\mathsf{T}} W^{-1} G)^{-1}. \tag{7}$$

Then, letting $H = (G^{\mathsf{T}} W^{-1} G)^{-1}$, we have the following weighted DOP metrics:

- Geometric DOP (GDOP) $= \sqrt{H_{11} + H_{22} + H_{33} + H_{44}}$;
- Horizontal DOP (HDOP) $= \sqrt{H_{11} + H_{22}}$;
- Vertical DOP (VDOP) $= \sqrt{H_{33}}$;
- Positional DOP (PDOP) $= \sqrt{H_{11} + H_{22} + H_{33}}$;
- Time DOP (TDOP) $= \sqrt{H_{44}}$.

C. Utility functions and equivalence of utility

For a certain mask angle and constellation setting, DOP varies with the time and user location. Figure 1 shows the empirical cumulative distribution functions (CDFs) of GDOP values for two scenarios: (a) a single constellation with a low mask angle and (b) two constellations with high mask angles. As can be seen, a higher mask angle pushes the CDF curve to the right and a lower mask angle pulls the CDF curve to the left. In addition, the mask angle also slightly affects the shape of the CDF curve: the CDF curve of two constellations with 15° mask is steeper than that of one constellation with 5° mask. This phenomenon indicates that the DOP values for multiple constellations usually have a smaller deviation than those for a single constellation. Therefore, no matter how much the mask angle is, hardly can the CDF of DOP values for multiple constellations exactly match that for a single constellation.

In theoretical analysis, we use a lower bound on the expectation of DOP as a utility function because it can indicate the expectation of DOP, and also because we can obtain a closed-form expression of it.

In simulation results, we consider a utility function that is more complex and direct than the lower bound on the expectation of DOP. We redefine the equivalence of utility in (2) as achieving the minimum distance between two CDFs:

$$\alpha^* = \arg\min_{\alpha} \delta\big(F_{n,\alpha}(x), F_{n_0,\alpha_0}(x)\big), \tag{8}$$

where $F_{n,\alpha}(x)$ is the empirical CDF of DOP values for a total of n satellites and a mask angle of α, and $\delta(F_1(x), F_2(x))$ is the distance between two empirical CDFs $F_1(x)$ and $F_2(x)$.

In this paper, we consider the following three distance functions:

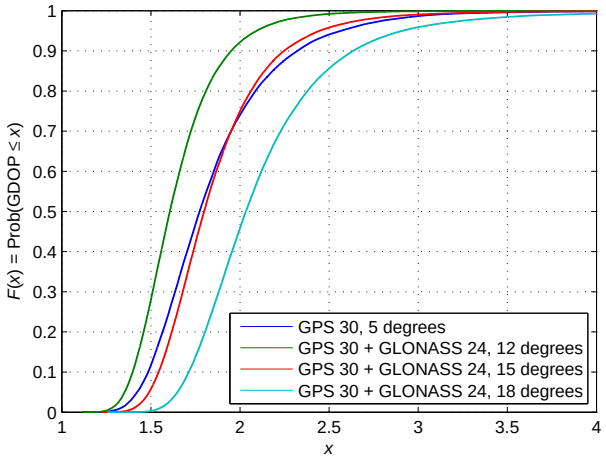

Fig. 1. Empirical CDF of GDOP values for a single constellation with a low mask angle versus that for multiple constellations with high mask angles. The CDF curve for multiple constellations cannot exactly match that for a single constellation.

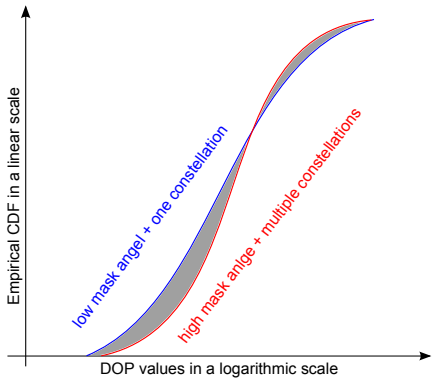

Fig. 2. The integral of relative difference between quantiles is equal to the area of the shaded region.

- Difference between sample means (equivalent to the expectation of DOP), which mainly captures position information of the CDF curve (to the left or to the right) but little information of the shape:

$$\delta_1(F_1(x), F_2(x)) = \left| \int_0^\infty x \, \mathrm{d}F_1(x) - \int_0^\infty x \, \mathrm{d}F_2(x) \right|; \tag{9}$$

- Integral of absolute difference between quantiles, which captures both the position and shape information, but inherently weights the upper tail more than the lower tail:

$$\delta_2(F_1(x), F_2(x)) = \int_0^1 \left| F_1^{-1}(y) - F_2^{-1}(y) \right| \mathrm{d}y; \tag{10}$$

- Integral of relative difference between quantiles (illustrated in Figrue 2), which captures both the position and shape information, with evenly weighting the upper and lower tails:

$$\delta_3(F_1(x), F_2(x)) = \int_0^1 \left| \log[F_1^{-1}(y)] - \log[F_2^{-1}(y)] \right| \mathrm{d}y, \tag{11}$$

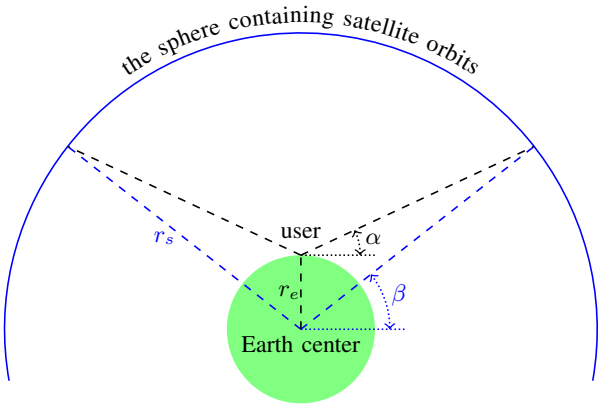

Fig. 3. Geometric method for calculating average number of satellites. α is the antenna mask angle, r_s is the radius of satellite orbit, and r_e is the Earth radius.

where the "relative difference" is due to the fact that $\log(a) - \log(b) = \log(1 + \frac{a-b}{b}) \approx \frac{a-b}{b}$ when $a \approx b$.

The above distance functions result in different optimal mask angles. However, Section IV-A2 will show that the differences between the optimal mask angles due to the distance functions are negligible.

III. Theoretical Analysis

This section theoretically analyzes the quantitative relationship between the antenna mask angle and the expectation of DOP. To simplify the analysis, we use circles as an approximation of the slightly elliptical satellite orbits, and assume the same range accuracy for all constellations. The analysis is based on the concept of *global average*, which means that the location of observers are uniformly and randomly chosen from the Earth surface. From an observer's point of view, global average also means that a satellites can be seen as uniformly distributed on the sphere containing their orbits. Therefore, we assume that satellites are uniformly, independently distributed on the sphere containing their orbits. The numerical results in Section IV will show that this assumption is valid.

A. Average number of satellites

Suppose that there are a total of n satellites in a GNSS constellation. As shown in Fig. 3, the average number of satellites is proportional to the area of the spherical cap above the angle β. By the law of sines, we have

$$\frac{\sin(\alpha + \pi/2)}{r_s} = \frac{\sin(\beta - \alpha)}{r_e}, \tag{12}$$

where α is the antenna mask angle, r_s is the radius of satellite orbit, and r_e is the Earth radius. Therefore, the angle β is given by

$$\beta = \alpha + \sin^{-1}\left(\frac{r_e}{r_s}\cos\alpha\right) = \alpha + \sin^{-1}(\kappa^{-1}\cos\alpha), \tag{13}$$

where $\kappa = r_s/r_e$ is the orbital radius normalized by the Earth radius. For GLONASS, GPS, Compass, and Galileo, $\kappa = 3.998$, 4.175, 4.375, and 4.645, respectively.

The average number of satellites in view is a function of n, α, and κ:

$$\begin{aligned} m(n, \alpha, \kappa) &= \frac{2\pi r_s(r_s - r_s\sin\beta)}{4\pi r_s^2} n \\ &= \frac{n}{2}\big(1 - \sin\big[\alpha + \sin^{-1}(\kappa^{-1}\cos\alpha)\big]\big). \end{aligned} \tag{14}$$

For multiple constellations, the average number of satellites in view is given by

$$\sum_{i=1}^{c} m(n_i, \alpha, \kappa_i), \tag{15}$$

where c is the number of constellations, n_i is the total number of satellites in constellation i, and κ_i the normalized orbital radius of constellation i, $i = 1, \ldots, c$.

B. Lower bound on expectation of DOP

The geometry matrix (3) can be rewritten as

$$G = \begin{pmatrix} \sqrt{1-u_1^2}\cos\theta_1 & \sqrt{1-u_1^2}\sin\theta_1 & u_1 & -1 \\ \vdots & \vdots & \vdots & \vdots \\ \sqrt{1-u_m^2}\cos\theta_m & \sqrt{1-u_m^2}\sin\theta_m & u_m & -1 \end{pmatrix}, \tag{16}$$

where $u_k = \sin\phi_k$ is the sine of the elevation angle of the kth satellite. Since the orbital radius is four times as large as the Earth radius, we consider a further approximation that, on average, the satellites are uniformly distributed on a sphere centered at the user. With such an approximate assumption, both u_k and θ_k are uniformly distributed [39]:

$$u_k \sim \mathcal{U}[\mu, 1], \tag{17}$$

$$\theta_k \sim \mathcal{U}[-\pi, \pi], \tag{18}$$

where $\mu = \sin\alpha$ and α is the antenna mask angle.

Under the assumption that all satellites have the same range accuracy, the expectation of DOP is derived from the diagonal elements of the matrix $\mathrm{E}\,H = \mathrm{E}[(G^\mathsf{T}G)^{-1}]$. Unfortunately, it is very difficult to evaluate $\mathrm{E}\,H$ analytically. Instead, we consider $[\mathrm{E}(G^\mathsf{T}G)]^{-1}$ here not only because it can be evaluated analytically, but also because it is proven to be a lower bound on $\mathrm{E}[(G^\mathsf{T}G)^{-1}]$, as stated by the following theorem.

Theorem 1 (Lower bound on expectation of random DOP matrix): For a random geometry matrix G defined in (16),

$$\mathrm{E}[(G^\mathsf{T}G)^{-1}] \succeq [\mathrm{E}(G^\mathsf{T}G)]^{-1}, \tag{19}$$

where the operator $X \succeq Y$ means that $X - Y$ is positive semidefinite.

A proof of this theorem is shown in the Appendix.

Rewriting the geometry matrix in (16) as $G = [g_1, g_2, g_3, g_4]$, where g_i, $i = 1, \ldots, 4$, are random vectors with a length of m, we have

$$\mathrm{E}(G^\mathsf{T}G) = [\mathrm{E}\, g_i^\mathsf{T} g_j]_{i,j=1,\ldots,4}. \tag{20}$$

For the distributions in (17) and (18), each element of $\mathrm{E}(G^{\mathsf{T}}G)$ is given by

$$\begin{aligned}\mathrm{E}\, g_1^{\mathsf{T}} g_1 = \mathrm{E}\, g_2^{\mathsf{T}} g_2 &= m\,\mathrm{E}(1-u_k^2)\,\mathrm{E}\cos^2\theta_k^2 \\ &= m\frac{2-\mu-\mu^2}{6}, \end{aligned} \tag{21}$$

$$\mathrm{E}\, g_3^{\mathsf{T}} g_3 = m\,\mathrm{E}(u_k^2) = m\frac{1+\mu+\mu^2}{3}, \tag{22}$$

$$\mathrm{E}\, g_4^{\mathsf{T}} g_4 = m, \tag{23}$$

$$\mathrm{E}\, g_3^{\mathsf{T}} g_4 = \mathrm{E}\, g_4^{\mathsf{T}} g_3 = -m\,\mathrm{E}\, u_k = -m\frac{1+\mu}{2}, \tag{24}$$

$$\begin{aligned}\mathrm{E}\, g_1^{\mathsf{T}} g_2 = \mathrm{E}\, g_2^{\mathsf{T}} g_1 &= \mathrm{E}\, g_1^{\mathsf{T}} g_3 = \mathrm{E}\, g_3^{\mathsf{T}} g_1 \\ &= \mathrm{E}\, g_1^{\mathsf{T}} g_4 = \mathrm{E}\, g_4^{\mathsf{T}} g_1 \\ &= \mathrm{E}\, g_2^{\mathsf{T}} g_3 = \mathrm{E}\, g_3^{\mathsf{T}} g_2 \\ &= \mathrm{E}\, g_2^{\mathsf{T}} g_4 = \mathrm{E}\, g_4^{\mathsf{T}} g_2 = 0, \end{aligned} \tag{25}$$

where the average number of satellites m is calculated from (15). The lower bound matrix is hence given by

$$\begin{aligned}&[\mathrm{E}(G^{\mathsf{T}}G)]^{-1} \\ &= \frac{1}{m}\begin{pmatrix} \frac{2-\mu-\mu^2}{6} & 0 & 0 & 0 \\ 0 & \frac{2-\mu-\mu^2}{6} & 0 & 0 \\ 0 & 0 & \frac{1+\mu+\mu^2}{3} & -\frac{1+\mu}{2} \\ 0 & 0 & -\frac{1+\mu}{2} & 1 \end{pmatrix}^{-1} \\ &= \frac{2}{m(1-\mu)}\begin{pmatrix} \frac{3}{2+\mu} & 0 & 0 & 0 \\ 0 & \frac{3}{2+\mu} & 0 & 0 \\ 0 & 0 & \frac{6}{1-\mu} & 3 \\ 0 & 0 & 3 & \frac{2(1+\mu+\mu^2)}{1-\mu} \end{pmatrix}. \end{aligned} \tag{26}$$

Therefore, we obtain the lower bound on the expectation of the five DOP metrics:

$$\mathrm{E}(\mathrm{GDOP}^2) \geq \frac{4}{m}\cdot\frac{9+(1+\mu+\mu^2)(2+\mu)}{(2+\mu)(1-\mu)^2}, \tag{27}$$

$$\mathrm{E}(\mathrm{HDOP}^2) \geq \frac{4}{m}\cdot\frac{3}{(2+\mu)(1-\mu)}, \tag{28}$$

$$\mathrm{E}(\mathrm{VDOP}^2) \geq \frac{4}{m}\cdot\frac{3}{(1-\mu)^2}, \tag{29}$$

$$\mathrm{E}(\mathrm{PDOP}^2) \geq \frac{4}{m}\cdot\frac{9}{(2+\mu)(1-\mu)^2}, \tag{30}$$

$$\mathrm{E}(\mathrm{TDOP}^2) \geq \frac{4}{m}\cdot\frac{1+\mu+\mu^2}{(1-\mu)^2}, \tag{31}$$

where $\mu = \sin\alpha$, and α is the antenna mask angle.

Figure 4 shows the lower bound on expectation of GDOP calculated using (27) for three constellation settings: 30 GPS satellites, 30 GPS + 24 GLONASS satellites, and 30 GPS + 24 GLONASS + 27 Galileo satellites. It can be seen that two constellations can match the GDOP performance of one with a mask angle of approximately 14°, and three constellations can match the GDOP performance of one with a mask angle of approximately 20°.

Figure 5 shows relationship between the optimal antenna mask angle and the total number of satellites for achieving GDOP, HDOP, VDOP, and TDOP of the baseline geometry. It can be seen that given a 15° mask angle, 44 satellites are required to achieve the baseline HDOP performance, 57

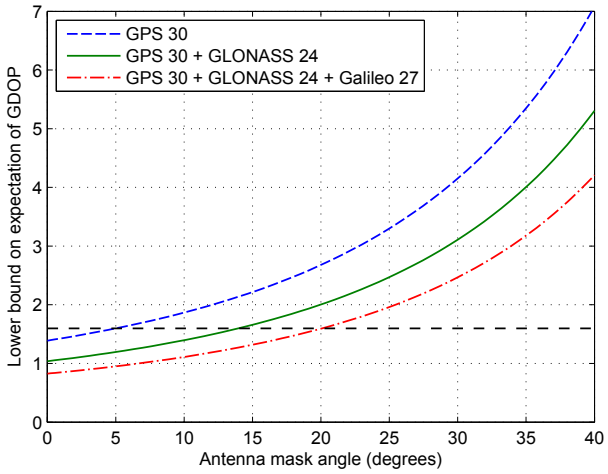

Fig. 4. Lower bound on expectation of GDOP calculated using (27) for one constellation comprised of 30 satellites, two constellations comprised of 54 satellites, and three constellations comprised of 84 satellites.

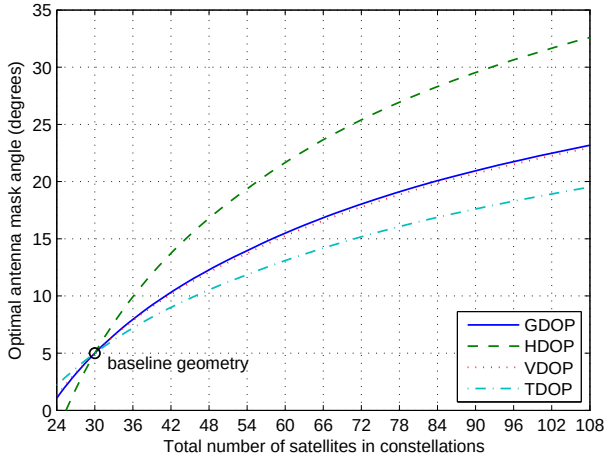

Fig. 5. The optimal antenna mask angle as a function of the total number of satellites for achieving GDOP, HDOP, VDOP, and TDOP of the baseline geometry.

satellites are required to achieve the baseline GDOP and VDOP performance, and 71 satellites are required to achieve the baseline TDOP performance. This shows that HMMA with multiple constellations is more beneficial to users interested in positioning accuracy (especially horizontal accuracy) than users interested in time transfer accuracy. This phenomenon is due to the fact that TDOP is much smaller than VDOP at a low mask angle, but TDOP is approximately equal to VDOP at a very high mask angle, as shown by (29) and (31). With an increasing mask angle, TDOP increases much faster than VDOP does.

Figure 5 also shows that the optimal mask angles to achieve the baseline VDOP and GDOP performance are very close. The first reason is that VDOP values are usually larger than HDOP and TDOP values, and thus dominate GDOP values. The second reason is that for an increasing mask angle, the HDOP value increases slower than the VDOP value, while the TDOP value increases faster than the VDOP value. The

difference between the increasing slopes of HDOP and TDOP approximately compensate each other, leaving the GDOP values almost only affected by the VDOP values.

Moreover, the concavity of all the curves in Fig. 5 implies diminishing marginal utility: the gain of mask angle due to adding one more satellite decreases as the total number of satellites increases.

IV. Numerical Results

In this section, we validate our theoretical analysis in Section III using numerical simulations. We use real GNSS satellite orbits based on broadcast almanacs or planned orbits. We generate a global user grid in which users are nearly evenly distributed on the Earth, as shown in Fig. 6. Satellites are selected at random out of the full constellation sets regardless of the user locations. DOP values are calculated at each of the user locations at different epochs based on the satellite visibility with a certain mask angle.

A. Simulation settings

All the results presented in this section are based on the simulation setting listed below.

- Orbit parameters:
  - GPS: broadcast almanacs of 30 usable GPS satellites on 23 January 2013.
  - GLONASS: broadcast almanacs of 24 active GLONASS-M satellites on 23 January 2013.
  - Galileo: planned orbits of 27 Galileo satellites [40].
  - Compass: planned orbits of 27 Compass middle earth orbiting (MEO) satellites [41].
- Baseline geometry: the GPS constellation of 30 satellites with a 5° mask angle.
- Constellation selection strategy for a total of n satellites:

  $24 \le n \le 30$: n randomly selected GPS satellites;
  $30 < n \le 54$: 30 GPS satellites and $(n-30)$ randomly selected GLONASS satellites;
  $54 < n \le 81$: 30 GPS satellites, 24 GLONASS satellites and $(n-54)$ randomly selected Galileo satellites;
  $81 < n \le 108$: 30 GPS satellites, 24 GLONASS satellites, 27 GLONASS satellites, and $(n-81)$ randomly selected Compass satellites.
- Temporal sampling: 1 sample per 29 minutes over 2 days.
- Spatial sampling: 1807 points nearly evenly distributed on the Earth, as shown in Fig. 6.
- Range accuracy:

  Model 1: the same range accuracy for all constellations.
  Model 2: 6 meters for GPS, Galileo, and Compass; 8 meters for GLONASS (explained below).
- Distance function: δ_1 defined in (9) (explained below).

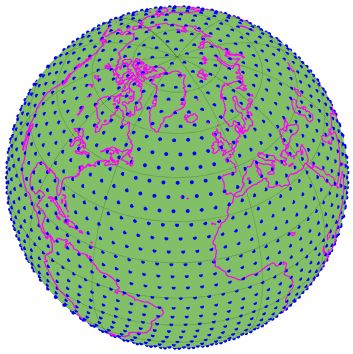

Fig. 6. DOP values are computed for 1807 points nearly evenly distributed on the Earth. The spherical distance between any two neighbor points is roughly 5°.

1) Constellation-specific range error models: In order to see how range accuracy affect optimal mask angle, this section considers the following constellation-specific range error model:

- Signal-in-space (SIS) errors: 3 meters for GPS [8], Galileo, and Compass; 6 meters for GLONASS.
- Atmospheric propagation modeling errors: 6 meters [8].
- Receiver noise and multipath: 1 meter for GPS [8], Galileo, and Compass; 2 meters for GLONASS.
- Total pseudorange measurement errors: 6 meters for GPS, Galileo, and Compass; 8 meters for GLONASS.

In the above list, Galileo and Compass are arbitrarily assumed to be on par with GPS. GLONASS is assumed to have a worse range accuracy because the GLONASS SIS errors are roughly twice as large as those of GPS [35], [36], and the chip rate of GLONASS civil signals is half of the chip rate of GPS, Galileo, and Compass civil signals.

In fact, Galileo and Compass have not yet been fully operational and their SIS accuracy performance is unknown. Today's GPS SIS accuracy is actually much better than 3 meters [34]. The ionospheric errors for a single-frequency receiver can be highly variable depending on the user location and satellite elevation angle. In addition, the noise and multipath can also vary with the satellite elevation angle [42]. Nevertheless, in this paper, the main purpose of considering weighted DOP in simulations is to check whether range accuracy can significantly affect the optimal mask angle. Since a sophisticated, accurate range error model is not necessary for this purpose (and not even possible because the Galileo and Compass SIS accuracy performance is unknown), we use this very simple error model despite its crudeness and inaccuracy.

2) Choosing a distance function: In Section II-C, we have proposed three functions for quantifying the distance between two CDFs. These distance functions result in different optimal mask angles. We must understand how the distance functions affect the optimal mask angle and decide which distance function to use in our simulations.

Table I compares the optimal mask angles obtained using the distance functions. It can be seen that the optimal mask angle obtained from the three distance functions differ by up to 0.3°. Considering this negligible difference, the results and discussion in the rest of this section will be based upon the

TABLE I
COMPARISON OF THE OPTIMAL MASK ANGLES OBTAINED USING THE THREE DISTANCE FUNCTIONS.

Distance function	Mask angles (°) to achieve the baseline GDOP performance	
	54 satellites	81 satellites
δ_1 defined in (9)	14.84	21.06
δ_2 defined in (10)	14.89	20.96
δ_3 defined in (11)	14.77	20.80

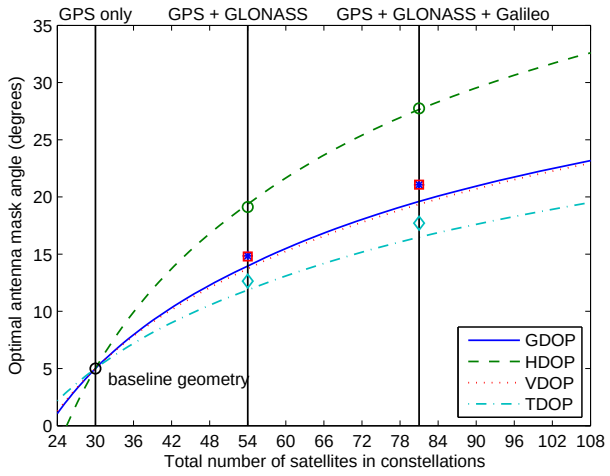

Fig. 7. Comparison between theoretical and numerical results. The markers show the optimal mask angles from the simulation results using range accuracy model 1. The theoretical equal-performance curves are the same as Fig. 5. The numerical results are consistent with our theoretical analysis.

distance function δ_1 defined in (9)—difference between sample means.

B. Validation of our theoretical analysis

Figure 7 compares theoretical and numerical results. The markers show the optimal mask angles from the simulation results using range accuracy model 1. The theoretical equal-performance curves are the same as Fig. 5. Although the theoretical analysis assumes randomly-distributed satellites whereas the simulations use actual or planned orbits, the numerical results are consistent with our theoretical analysis, with less than 1.5-degree difference in optimal mask angles. This comparison validates our theoretical analysis, and demonstrates that our lower bound on expectation of DOP is a valid performance indicator.

C. Optimal mask angles for different DOP metrics and different range error models

Table II compares the optimal mask angles for five different DOP metrics and under two different assumptions of range accuracy. It can be seen that the incorporation of 24 GLONASS satellites can matches the baseline GDOP performance with 10° higher mask if GLONASS range accuracy can be assumed to be as good as GPS. If the range accuracy model 2 is used, GPS + GLONASS can match the GDOP performance of GPS-only with 7° higher mask.

TABLE II
OPTIMAL MASK ANGLES FOR DIFFERENT DOP METRICS, CONSTELLATION SETTINGS, AND RANGE ACCURACY MODELS.

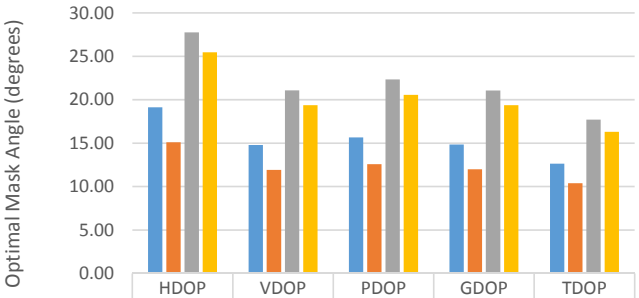

	HDOP	VDOP	PDOP	GDOP	TDOP
54 satellites Model 1	19.12	14.79	15.67	14.84	12.64
54 satellites Model 2	15.10	11.92	12.58	11.99	10.38
81 satellites Model 1	27.75	21.08	22.34	21.06	17.71
81 satellites Model 2	25.46	19.37	20.56	19.37	16.31

- Constellations:
  - 54 sats: 30 GPS and 24 GLONASS satellites;
  - 81 sats: 30 GPS, 24 GLONASS, and 27 Galileo satellites.
- Range accuracy models:
  - Model 1: the same range accuracy, 6 meters, for all constellations;
  - Model 2: 6 meters for GPS and Galileo, and 8 meters for GLONASS.

Table II shows that with increased number of satellites, a high mask angle can match the HDOP performance more easily than the TDOP performance. Table II also shows that the optimal mask angles to achieve the baseline VDOP and GDOP performance are very close. These observations highly agree with our theoretical analysis in Section III.

D. Contour plots of DOP values as a comprehensive guideline on choosing the optimum mask angle

All the above optimal mask angles are based on achieving the performance of the predefined baseline geometry with multiple constellations comprised of either 54 or 81 satellites. The contour plots of HDOP, VDOP, and TDOP values shown in Fig. 8 provide a comprehensive guideline on finding the optimum mask angle to achieve the performance of a different baseline geometry with an arbitrary number of satellites. For example, if the baseline geometry is a single constellation of 24 satellites with a 7.5° mask angle, with 60 satellites in multiple constellations, we can increase the mask angle to 28°, 24°, and 21° to match the HDOP, VDOP, and TDOP performance, respectively.

Like Table II, the contour plots in Fig. 8 shows that the mask angle should be raised less to achieve the baseline TDOP performance, compared to achieving the baseline HDOP and VDOP performance. Therefore, using HMAAs is more beneficial to users interested in positioning accuracy (especially horizontal accuracy) than users interested in time transfer accuracy.

Moreover, both Fig. 8 and Table II demonstrate diminishing marginal utility: the gain of mask angle due to adding one

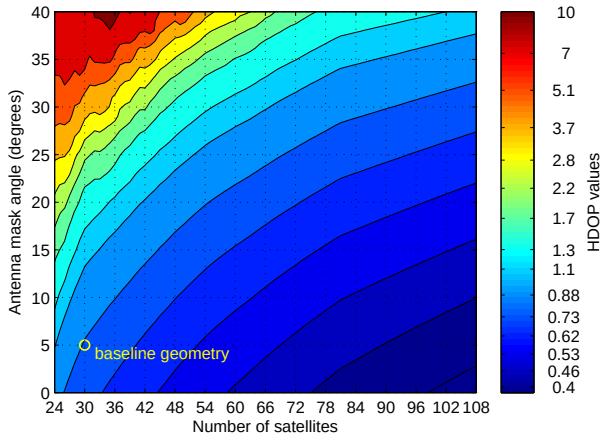

(a) Contour plots of HDOP values

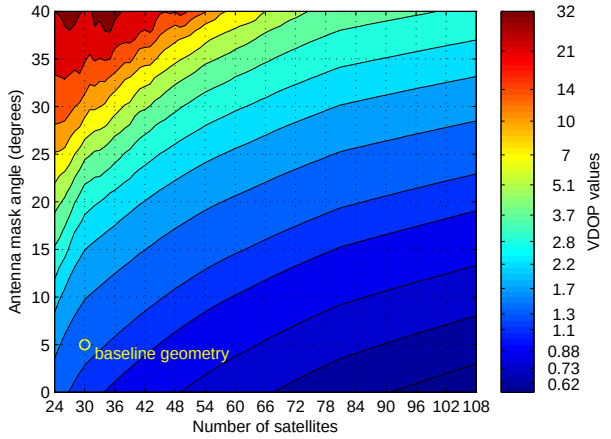

(b) Contour plots of VDOP values

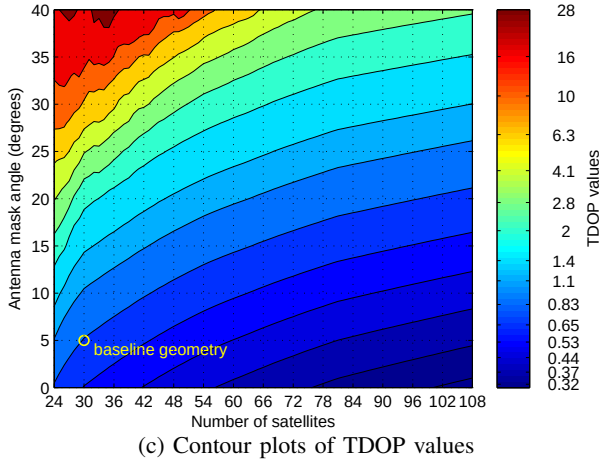

(c) Contour plots of TDOP values

Fig. 8. Contour plots of HDOP, VDOP, and TDOP values. The isolines show how much the mask angle can be raised to match certain DOP performance. Assume the same range accuracy for all constellations.

more satellite decreases as the total number of satellites increases.

E. Impact to Users at Different Latitudes

It has been well known that the vertical accuracy of GPS deteriorates at high latitudes due to lack of satellites at high elevation angles [43], [44]. For high-latitude GNSS users,

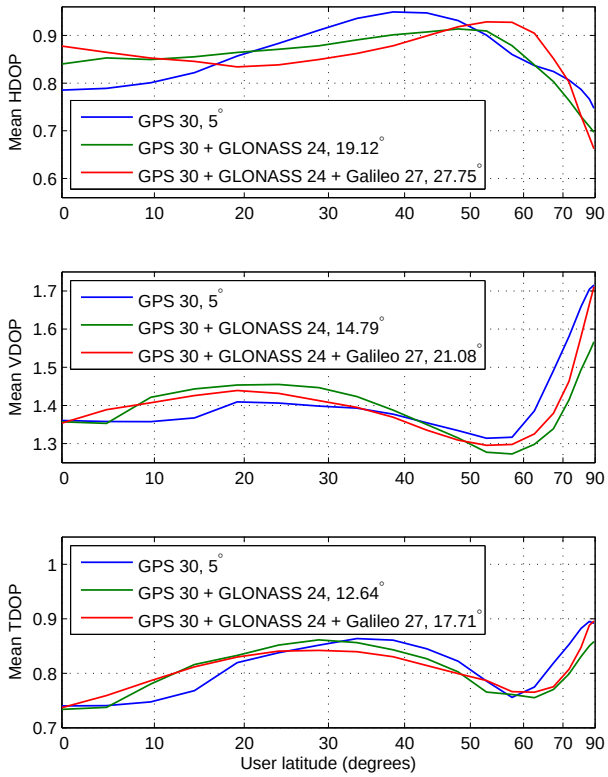

Fig. 9. Mean HDOP, VDOP, and TDOP values observed by users at different latitudes.

using HMAA is a double-edged sword: on one hand, additional satellites offered by multiple constellations can improve the geometry; on the other hand, the high mask angle rejects many satellites at low elevation angles, and thus worsens the geometry. Therefore, a question that need be answered is how HMAAs affect the positioning performance at high latitudes. An more generalized question is how HMAAs affect the DOP performance observed by users at different latitudes.

Figure 9 shows the answer to the generalized question. In each subfigure, the mask angles for multiple constellations are chosen to match the globally-averaged DOP performance of the baseline geometry. As can be seen, using HMAAs is slightly more beneficial to high-latitude users than mid- and low-latitude users, especially in terms of VDOP and TDOP performance. However, this is partially due to the relatively high inclination of GLONASS orbits because the introduction of the Galileo constellation actually worsens the VDOP and TDOP performance for high-latitude users. On the whole, using HMAAs does not result in a significant change of performance for users at different latitudes.

V. Conclusion

In this paper, we systematically studied a new method to mitigate low-elevation multipath and jamming interference signals—using HMAAs and multiple GNSS constellations. Our goal is to find the highest mask angle such that the accuracy performance of multiple constellations can match that of a single constellation with low mask angle antennas. We achieved this goal via two approaches:

- Theoretical analysis based on a novel lower bound on expectation of DOP;
- Numerical simulations with respect to different constellation settings, different DOP metrics, and different range accuracy models.

The two approaches lead to consistent results, from which the following conclusions can be drawn.

- GPS + GLONASS can match performance of GPS with 5–14° higher mask, and GPS + GLONASS + Galileo can match performance of GPS with 11–23° higher mask.
- The optimal mask angle mainly depends on the total number of satellites, the performance measure (HDOP, VDOP, etc.), and the range error model.
- Diminishing marginal utility: the gain of mask angle due to adding one more satellite always decreases as the total number of satellites increases.
- This method is more beneficial to users interested in positioning accuracy (especially horizontal accuracy) than users interested in time transfer accuracy.
- This method does not significantly influence the positioning performance observed by users at different latitudes.

In general, using HMAAs is a practical, effective method for multi-constellation GNSS users to mitigate multipath and jamming interference. The theory and numerical results presented in this paper provide guidelines on designing HMAAs and using this method in practice.

Appendix
Proof of Theorem 1

There are a few approaches to proving Theorem 1. One of the simplest proofs is based on recent results on the Cauchy–Schwarz inequality for the expectation of random matrices [45], [46]:

Lemma 1 (Cauchy–Schwarz inequality [45], [46]): Let $A \in \mathbb{R}^{n\times p}$ and $B \in \mathbb{R}^{n\times p}$ be random matrices such that $\mathrm{E}\,\|A\|^2 < \infty$, $\mathrm{E}\,\|B\|^2 < \infty$, and $\mathrm{E}(A^{\mathsf{T}}A)$ is non-singular. Then

$$\mathrm{E}(B^{\mathsf{T}}B) \succeq \mathrm{E}(B^{\mathsf{T}}A)[\mathrm{E}(A^{\mathsf{T}}A)]^{-1}\,\mathrm{E}(A^{\mathsf{T}}B). \tag{32}$$

With the substitutions $A = G$ and $B = G(G^{\mathsf{T}}G)^{-1}$ into the above inequality, we have

$$U = \mathrm{E}[(G^{\mathsf{T}}G)^{-1}] \succeq V = [\mathrm{E}(G^{\mathsf{T}}G)]^{-1}, \tag{33}$$

which already proves Theorem 1.

Since the diagonal elements of a positive semidefinite matrix must be non-negative, we have

$$U_{ii} \geq V_{ii}, \quad \forall i = 1, \ldots, dN_S, \tag{34}$$

where $U = [U_{ij}]$ and $V = [V_{ij}]$. In particular, the expectation of GDOP, $\sqrt{\mathrm{trace}(U)}$, has a lower bound $\sqrt{\mathrm{trace}(V)}$.

Like DOP metrics, the lower bound also has the non-degeneration property, i.e.,

$$[\mathrm{E}(G^{\mathsf{T}}G)]^{-1} \succeq \left[\mathrm{E}\left(\begin{bmatrix}G\\X\end{bmatrix}^{\mathsf{T}}\begin{bmatrix}G\\X\end{bmatrix}\right)\right]^{-1}, \tag{35}$$

for any random matrix $X \in \mathbb{R}^{n\times dN_S}$, $n \in \mathbb{N}$. This property indicates that adding more satellites always improves geometry.

Proof: Expand the right side as $[\mathrm{E}(G^{\mathsf{T}}G)+\mathrm{E}(X^{\mathsf{T}}X)]]^{-1}$. Since $\mathrm{E}(G^{\mathsf{T}}G)] + \mathrm{E}(X^{\mathsf{T}}X) \succeq \mathrm{E}(G^{\mathsf{T}}G)] \succ \mathbf{0}$, we have $[\mathrm{E}(G^{\mathsf{T}}G)]^{-1} \succeq [\mathrm{E}(G^{\mathsf{T}}G)] + \mathrm{E}(X^{\mathsf{T}}X)]^{-1}$ [47]. ■

References

[1] C. R. Drane and C. Rizos, *Positioning Systems in Intelligent Transportation Systems*. Norwood, MA, USA: Artech House, Inc., 1998.

[2] S. T. S. Thong, C. T. Han, and T. A. Rahman, "Intelligent fleet management system with concurrent GPS & GSM real-time positioning technology," in *Proceedings of the 7th International Conference on ITS Telecommunications (ITST '07)*, June 2007, pp. 1–6.

[3] G. Mintsis, S. Basbas, P. Papaioannou, C. Taxiltaris, and I. Tziavos, "Applications of GPS technology in the land transportation system," *European Journal of Operational Research*, vol. 152, no. 2, pp. 399–409, 2004.

[4] J.-P. Clarke, "The role of advanced air traffic management in reducing the impact of aircraft noise and enabling aviation growth," *Journal of Air Transport Management*, vol. 9, no. 3, pp. 161–165, 2003, aviation and sustainability.

[5] A. Grant, P. Williams, N. Ward, and S. Basker, "GPS jamming and the impact on maritime navigation," *The Journal of Navigation*, vol. 62, pp. 173–187, 4 2009.

[6] A. Komjathy, V. U. Zavorotny, P. Axelrad, G. H. Born, and J. L. Garrison, "GPS signal scattering from sea surface: Wind speed retrieval using experimental data and theoretical model," *Remote Sensing of Environment*, vol. 73, no. 2, pp. 162 – 174, 2000.

[7] M. S. Braasch, "Multipath effects," in *Global Positioning System: Theory and Applications*, B. Parkinson, J. Spilker, P. Axelrad, and P. Enge, Eds. Washington, DC: American Institute of Aeronautics and Astronautics, 1996, vol. I, pp. 547–568.

[8] P. Misra and P. Enge, *Global Positioning System: Signals, Measurements, and Performance*, 2nd ed. Lincoln, MA: Ganga-Jamuna Press, 2006.

[9] S. Pullen and G. X. Gao, "GNSS jamming in the name of privacy: Potential threat to GPS aviation," *Inside GNSS*, Mar. 2012.

[10] J. M. Tranquilla, J. P. Carr, and H. M. Al-Rizzo, "Analysis of a choke ring groundplane for multipath control in Global Positioning System (GPS) applications," *IEEE Transactions on Antennas and Propagation*, vol. 42, no. 7, pp. 905–911, Jul. 1994.

[11] W. Kunysz, "High performance GPS pinwheel antenna," in *Proceedings of the 13th International Technical Meeting of the Satellite Division of the Institute of Navigation (ION GPS 2000)*, Salt Lake City, UT, Sep. 2000, pp. 2506–2511.

[12] A. Kerkhoff, R. B. Harris, C. P. Petersen, and A. Pickard, "Modifications to GPS reference station antennas to reduce multipath," in *Proceedings of the 23rd International Technical Meeting of the Satellite Division of the Institute of Navigation (ION GNSS 2010)*, Portland, OR, Sep. 2010, pp. 866–878.

[13] C. C. Counselman, "Array antennas for DGPS," *IEEE Aerospace and Electronic Systems Magazine*, vol. 13, no. 12, pp. 15–19, Dec. 1998.

[14] J. K. Ray, "Mitigation of gps code and carrier phase multipath effects using a multi-antenna system," Ph.D. dissertation, University of Calgary, Mar. 2000.

[15] A. J. Van Dierendonck, P. Fenton, and T. Ford, "Theory and performance of narrow correlator spacing in a GPS receiver," *NAVIGATION*, vol. 39, no. 3, Fall 1992.

[16] L. Garin, F. van Diggelen, and J.-M. Rousseau, "Strobe & edge correlator multipath mitigation for code," in *Proceedings of the 9th International Technical Meeting of the Satellite Division of the Institute of Navigation (ION GPS 1996)*, Kansas City, MO, Sep. 1996, pp. 657–664.

[17] R. Hatch, "The synergism of GPS code and carrier measurements," in *International Geodetic Symposium on Satellite Doppler Positioning*, 1983, pp. 1213–1231.

[18] C. J. Comp and P. Axelrad, "Adaptive snr-based carrier phase multipath mitigation technique," *IEEE Transactions on Aerospace and Electronic Systems*, vol. 34, no. 1, pp. 264–276, Jan. 1998.

[19] C. Pinana-Diaz, R. Toledo-Moreo, D. Betaille, and A. Gomez-Skarmeta, "GPS multipath detection and exclusion with elevation-enhanced maps," in *2011 14th International IEEE Conference on Intelligent Transportation Systems (ITSC)*, Oct. 2011, pp. 19–24.

[20] M. V. Tazebay and A. N. Akansu, "Adaptive subband transforms in time-frequency excisers for DSSS communications systems," *IEEE Transactions on Signal Processing*, vol. 43, no. 11, pp. 2776–2782, Nov. 1995.

[21] A. S. Ayaz, R. Bauernfeind, T. Pany, and B. Eissfeller, "Time-frequency based intentional interference suppression techniques in GNSS receivers," in *Proceedings of the 25th International Technical Meeting of the Satellite Division of the Institute of Navigation (ION GNSS 2012)*, Nashville, TN, Sep. 2012.

[22] G. X. Gao, L. Heng, A. Hornbostel, H. Denks, M. Meurer, T. Walter, and P. Enge, "DME/TACAN interference mitigation for GNSS: Algorithms and flight test results," *GPS Solutions*, vol. 17, no. 4, pp. 561–573, Oct. 2013.

[23] D.-J. Moelker and Y. Bar-Ness, "An optimal array processor for GPS interference cancellation," in *15th AIAA/IEEE Digital Avionics Systems Conference*, Oct. 1996, pp. 285–291.

[24] D. De Lorenzo, J. Gautier, J. Rife, P. Enge, and D. Akos, "Adaptive array processing for GPS interference rejection," in *Proceedings of the 18th International Technical Meeting of the Satellite Division of the Institute of Navigation (ION GNSS 2005)*, Long Beach, CA, Sep. 2005, pp. 618–627.

[25] Y.-H. Chen, J.-C. Juang, J. Seo, S. Lo, D. M. Akos, D. De Lorenzo, and P. Enge, "Design and implementation of real-time software radio for anti-interference GPS/WAAS sensors," *Sensors*, vol. 12, no. 10, pp. 13 417–13 440, 2012.

[26] D. De Lorenzo, "Navigation accuracy and interference rejection for GPS adaptive antenna arrays," Ph.D. dissertation, Stanford University, 2007.

[27] S. Pullen, G. X. Gao, C. Tedeschi, and J. Warburton, "The impact of uninformed RF interference on GBAS and potential mitigations," in *Proceedings of the 2012 International Technical Meeting of the Institute of Navigation (ION ITM 2012)*, Newport Beach, CA, Jan. 2012, pp. 780–789.

[28] F. N. Bauregger, "Novel anti-jam antennas for airborne GPS navigation," Ph.D. dissertation, Stanford University, 2003.

[29] R. B. Langley, "Dilution of precision," *GPS world*, vol. 10, no. 5, pp. 52–59, 1999.

[30] J. Spilker, "Satellite constellation and geometric dilution of precision," in *Global Positioning System: Theory and Applications*, B. Parkinson, J. Spilker, P. Axelrad, and P. Enge, Eds. Washington, DC: American Institute of Aeronautics and Astronautics, 1996, vol. I, pp. 177–208.

[31] H. Sairo, D. Akopian, and J. Takala, "Weighted dilution of precision as quality measure in satellite positioning," *IEE Proceedings Radar, Sonar and Navigation*, vol. 150, no. 6, pp. 430–436, Dec. 2003.

[32] C. Seynat, A. Kealy, and K. Zhang, "A performance analysis of future global navigation satellite systems," *Journal of Global Positioning Systems*, vol. 3, no. 1–2, pp. 232–241, 2004.

[33] M. Zhang and J. Zhang, "A fast satellite selection algorithm: Beyond four satellites," *IEEE Journal of Selected Topics in Signal Processing*, vol. 3, no. 5, pp. 740–747, Oct. 2009.

[34] L. Heng, G. X. Gao, T. Walter, and P. Enge, "Statistical characterization of GPS signal-in-space errors," in *Proceedings of the 2011 International Technical Meeting of the Institute of Navigation (ION ITM 2011)*, San Diego, CA, Jan. 2011, pp. 312–319.

[35] ——, "Statistical characterization of GLONASS broadcast ephemeris errors," in *Proceedings of the 24th International Technical Meeting of the Satellite Division of the Institute of Navigation (ION GNSS 2011)*, Portland, OR, Sep. 2011, pp. 3109–3117.

[36] ——, "Statistical characterization of GLONASS broadcast clock errors and signal-in-space errors," in *Proceedings of the 2012 International Technical Meeting of the Institute of Navigation (ION ITM 2012)*, Newport Beach, CA, Jan. 2012, pp. 1697–1707.

[37] U.S. Coast Guard Navigation Center, *Navstar GPS User Equipment Introduction*, Sep. 1996. [Online]. Available: http://www.navcen.uscg.gov/pubs/gps/gpsuser/gpsuser.pdf

[38] G. Hein, "Gnss interoperability: Achieving a global system of systems or 'does everything have to be the same?'," *Inside GNSS*, vol. 1, no. 1, Jan. 2006.

[39] E. W. Weisstein, "Sphere point picking," *MathWorld—A Wolfram Web Resource*. [Online]. Available: http://mathworld.wolfram.com/SpherePointPicking.html

[40] European Union, *European GNSS (Galileo) Open Service Signal In Space Interface Control Document*, Sep. 2010.

[41] China Satellite Navigation Office, *Report on the Development of BeiDou Navigation Satellite System*, Dec. 2012.

[42] A. Jahn, H. Bischl, and G. Heiss, "Channel characterisation for spread spectrum satellite communications," in *IEEE 4th International Symposium on Spread Spectrum Techniques and Applications*, vol. 3, Sep. 1996, pp. 1221–1226.

[43] S. Dosso, M. Vinnins, G. Lachapelle, G. Heard, and E. Cannon, "High latitude attitude," *GPS World*, Oct. 2003.

[44] G. X. Gao, L. Heng, T. Walter, and P. Enge, "Breaking the ice: Navigating in the Arctic," in *Proceedings of the 24th International Technical Meeting of the Satellite Division of the Institute of Navigation (ION GNSS 2011)*, Portland, OR, Sep. 2011, pp. 3767–3772.

[45] G. Tripathi, "A matrix extension of the Cauchy-Schwarz inequality," *Economics Letters*, vol. 63, no. 1, pp. 1–3, 1999.

[46] P. Lavergne, "A Cauchy-Schwarz inequality for expectation of matrices," Simon Fraser University, Tech. Rep., Nov. 2008.

[47] R. A. Horn and C. R. Johnson, *Matrix Analysis*. Cambridge University Press, 1990.

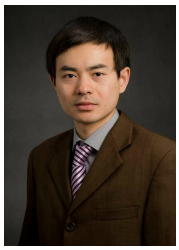

Liang Heng received the B.S. and M.S. degrees in electrical engineering from Tsinghua University, Beijing, China in 2006 and 2008. He received the PhD degree in electrical engineering from Stanford University in 2012. He is a postdoctoral research associate in the Department of Aerospace Engineering, University of Illinois at Urbana-Champaign. His research interests are cooperative navigation and satellite navigation. He is a member of the Institute of Electrical and Electronics Engineers (IEEE) and the Institute of Navigation (ION).

Todd Walter is a senior research engineer in the Department of Aeronautics and Astronautics at Stanford University. He received his Ph.D. from Stanford and is currently working on the Wide Area Augmentation System (WAAS), defining future architectures to provide aircraft guidance, and working with the FAA and GPS Wing on assuring integrity on GPS III. Key early contributions include prototype development proving the feasibility of WAAS, significant contribution to WAAS MOPS, and design of ionospheric algorithms for WAAS. He is a fellow of the ION.

Per Enge is a Professor of Aeronautics and Astronautics at Stanford University, where he is the Vance and Arlene Coffman Professor in the School of Engineering. He directs the GPS Research Laboratory, which develops satellite navigation systems based on the Global Positioning System (GPS). He has been involved in the development of WAAS and LAAS for the FAA. Per has received the Kepler, Thurlow and Burka Awards from the ION for his work. He is an Elected Member of National Academy of Engineering, and also a Fellow of the IEEE and the ION. He received his PhD from the University of Illinois in 1983.

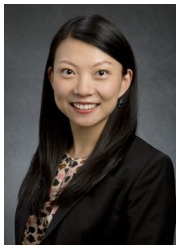

Grace Xingxin Gao received the B.S. degree in mechanical engineering and the M.S. degree in electrical engineering from Tsinghua University, Beijing, China in 2001 and 2003. She received the PhD degree in electrical engineering from Stanford University in 2008. From 2008 to 2012, she was a research associate at Stanford University. Since 2012, she has been with University of Illinois at Urbana-Champaign, where she is presently an assistant professor in the Aerospace Engineering Department. Her research interests are systems, signals, control, and robotics. She is a member of the IEEE and the ION.